Available online at www.sciencedirect.com

ScienceDirect

Geochimica et Cosmochimica Acta 295 (2021) 65–79

Geochimica et Cosmochimica Acta

www.elsevier.com/locate/gca

Underground production of ^{81}Kr detected in subsurface fluids

R. Purtschert [a,*], R. Yokochi [b], W. Jiang [d], Z.-T. Lu [d], P. Mueller [c], J. Zappala [c], E. Van Heerden [e,1], E. Cason [e], M. Lau [f,2], T.L. Kieft [g], C. Gerber [a,3], M.S. Brennwald [h], T.C. Onstott [f]

[a] *Climate and Environmental Physics and Oeschger Center for Climate Change Research, University of Bern, CH-3012 Bern, Switzerland*
[b] *Department of the Geophysical Sciences, The University of Chicago, Chicago, IL 60637 USA*
[c] *Physics Division, Argonne National Laboratory, Lemont, IL 60439, USA*
[d] *Hefei National Laboratory for Physical Sciences at the Microscale, CAS Center for Excellence in Quantum Information and Quantum Physics, The University of Science and Technology of China, Hefei 230026, China*
[e] *University of the Free State, Bloemfontein 9300, South Africa*
[f] *Department of Geoscience, Princeton University, Princeton, NJ 08544, USA*
[g] *Department of Biology, New Mexico Institute of Mining and Technology, Socorro, NM 87801, USA*
[h] *Eawag, Swiss Federal Institute of Aquatic Science and Technology, CH-8600 Dübendorf, Switzerland*

Received 2 February 2020; accepted in revised form 25 November 2020; available online 2 December 2020

Abstract

Radiokrypton dating using the long-lived natural isotope ^{81}Kr has been developed for determining the age of ancient groundwater. ^{81}Kr is attractive for this purpose because it is generally thought to be produced solely in the upper atmosphere. Its 229,000-year half-life, a spatially homogeneous distribution in the atmosphere, and the absence of anthropogenic sources makes it an ideal tracer to determine ages up to ~1.3 million years. As a noble gas, it is inert and thus not subject to interfering geochemical reactions that may alter the age information. We sought to date groundwater samples collected from deep (0.6–1.9 km) rock fractures in the Kaapvaal Craton, South Africa. Previous studies using other dating methods have estimated groundwater ages at these sites in the 1–100 million year range. Surprisingly, three of the four samples collected from flowing boreholes in gold and diamond mines showed ^{81}Kr isotopic abundances at 2–5 times the atmospheric value. This is the first time that underground production of ^{81}Kr has been detected, indicating that ^{81}Kr can be generated underground in measurable quantities in contrast to the long-held paradigm that such production is insignificant in natural rocks. A radionuclide production and release model is proposed in order to quantify the importance of different factors that affect the concentrations of ^{81}Kr in the groundwater. It is not only the high effective uranium content of the rock but also a higher ^{81}Kr fission yield than previously anticipated that are likely causing the elevated ^{81}Kr values in this case. In less extreme environments with average crustal composition (i.e. moderate U concentration), however, we anticipate that the underground production minimally affects groundwater ^{81}Kr dating as demonstrated.

* Corresponding author.
E-mail address: roland.purtschert@climate.unibe.ch (R. Purtschert).
[1] Present address: Centre for Water Sciences and Management, North West University, Potchefstroom, South Africa
[2] Present address: Institute of Deep-Sea Science and Engineering, Chinese Academy of Sciences, No. 28, Luhuitou Road, Sanya 572000, Hainan Province, PR China.
[3] Present address: Commonwealth Scientific and Industrial Research Organisation (CSIRO), Land and Water, PMB 2, Glen Osmond, SA 5064, Australia.

https://doi.org/10.1016/j.gca.2020.11.024

Keywords: Radiokrypton dating; Groundwater; Kapvaal craton; Fissiogenic production

1. INTRODUCTION

1.1. The ^{81}Kr dating method

Only a few tracers are available for dating groundwater on the time scale of one million years. The ^{4}He and ^{40}Ar/^{36}Ar methods are based on the accumulation of elements produced underground and the ^{36}Cl ($T_{1/2} = 301$ kyr) and ^{81}Kr ($T_{1/2} = 229$ kyr) methods are based on the radioactive decay in the subsurface (Aggarwal et al., 2013; Sturchio and Purtschert, 2013). Most of these methods provide only qualitative age information because they rely on knowledge about accumulation rates and secondary chemical dilution processes in the underground that are difficult to constrain. The ^{81}Kr method, the newest addition to this group (Jiang et al., 2012; Jiang et al., 2020), has been proposed as the optimal dating tool because as a noble gas, its results can be interpreted without complicated interfering geochemical reactions (Lu et al., 2014; Sturchio et al., 2014; Yokochi et al., 2019). Additionally, underground production has generally been thought to be negligible (see below). Secular equilibrium concentrations of ^{81}Kr in most geological environments had been estimated to be below 1% of the modern atmospheric concentration (percent Modern Krypton where 100 pMKr corresponds to $^{81}Kr/Kr = 9.3 \pm 0.3\ 10^{-13}$ (Zappala et al., 2020)). However, experimental evidence that confirm the low ^{81}Kr production and accumulation rates are scarce because of the limited number of ^{81}Kr case studies that have been carried out so far. The samples with lowest measured ^{81}Kr values have been found in Estonia, with < 5 pMKr (Gerber et al., 2017) and pMKr values ≤ 10 have been reported in the Guarani aquifer in Brazil, the Nubian Sandstone aquifer and the North China Plains (Aggarwal et al., 2015; Li et al., 2017; Matsumoto et al., 2018; Sturchio et al., 2014). New facilities with improved sensitivity for ^{81}Kr analysis are now operational (Dong et al., 2019; Jiang et al., 2020) and the ^{81}Kr method is expected to serve as one of the most common methods for dating very old groundwater (AGENCY, 2013). It is therefore of utmost importance to better constrain the production rate of ^{81}Kr in the subsurface. Undetected or underrated underground production of ^{81}Kr would lead to an underestimation of the inferred groundwater residence time.

2. GEOLOGIC SETTING AND SAMPLING METHODS

The Witwatersrand Basin lies within the Archaean Kaapvaal Craton of South Africa (Fig. 1) and is comprised of three supergroups, the 2.98–2.78 Gyr metasediments of the Witwatersrand Supergroup, the 2.7 Gyr metamorphosed basalt of the Ventersdorp Supergroup, and the sediments and volcanic strata of the 2.4–2.6 Gyr Transvaal Supergroup (Frimmel et al., 2005). The latter unconformably overlies the former and all unconformably overlie a 3.0–3.5 Gyr granite-greenstone basement (Nwaila et al., 2017)). The Witwatersrand Supergroup is comprised of a maximum of 8030 m of predominantly terrigenous sediment (Nwaila et al., 2017). In the region of Welkom on the southwestern margin of the basin (Fig. 1), in which three of the investigated mines (Beatrix and Masimong gold mines and Star Diamond mine) are located within 100 km distance to each other, mining is confined to narrow ore zones within the quartzites of the Witwatersrand Supergroup, which structurally dip to the northeast. Previous studies using noble gases and other dating methods have concluded residence times of the fracture fluids in Kaapvaal Craton of millions of years (Heard et al., 2018; Lippmann et al., 2003). The Finsch Diamond Mine is located approximately 400 km further west in the Transvaal Supergroup Ghaap dolomite, where the fracture fluid is in contact with a chemical (and thus neutron-flux) environment that is distinctly different from that of the other three mines.

At the time of this project the analyses of noble gas radionuclides required relatively large quantities of gas, equivalent to dissolved gas in 100–200 L of air-saturated water (ASW), free from atmospheric contamination.[4] As previous studies of stable noble gases have reported, most deep fracture water in the Witwatersrand Basin experienced degassing with depletion factors of up to 10 (Lippmann-Pipke et al., 2011; Lippmann et al., 2003), requiring even larger quantities of water from which gas was extracted using field gas extraction devices (Purtschert et al., 2013; Yokochi, 2016). In ideal cases of groundwater studies, water is extracted using a pump deeply submerged into a well. Because this was not possible in underground mines, packers were inserted into boreholes intersecting water-bearing fractures and used during water collection (Lau et al., 2016). However, even if the borehole installation is perfectly sealed, it remains possible that the fracture water was in contact with gas pockets within the fracture prior to discharge.

For this project, three sampling campaigns were carried out (Table 1). In 2012 three samples were collected with a membrane degassing device from the University of Bern, which was originally designed for large volume ^{39}Ar sampling (Purtschert et al., 2013). Another campaign was carried out in 2013 using the same device. Because of the very surprising results obtained in the first campaign and in order to exclude the possibility of any analytical interferences, one site (near 3 shaft of the Beatrix Gold Mine – Fig. 1) was resampled in 2016 with a smaller and more portable device constructed by the University of Chicago group (Yokochi, 2016). Additionally, air samples were

[4] in the meantime, the required sample volume could be lowered to 20–40 L (Jiang et al., 2020)

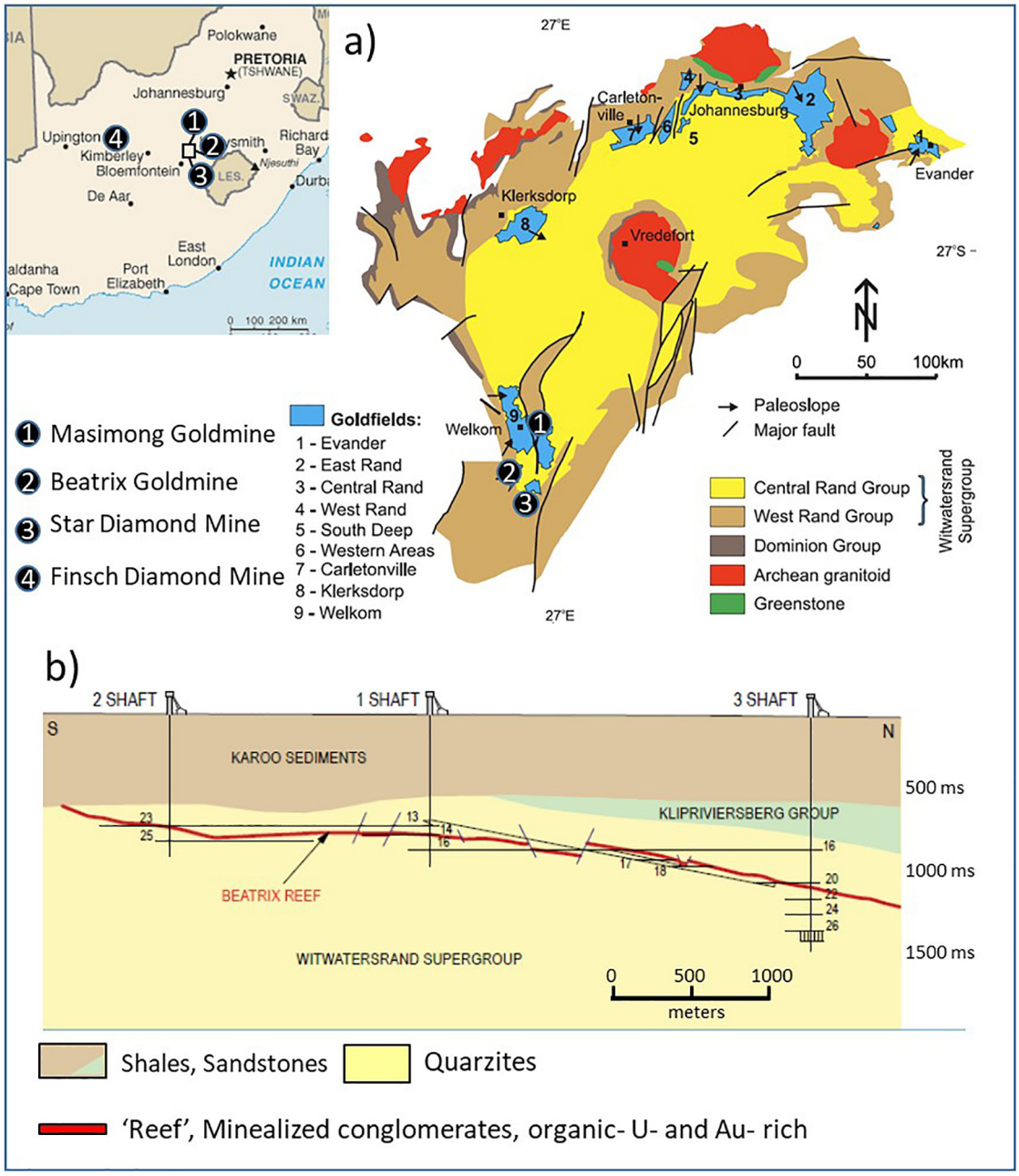

Fig. 1. a) Location of the mines investigated in this study. Mines (1–3), Beatrix, Star Diamond, and Masimong mines are located in the Witwatersrand Basin within the Welkom goldfields. The geology is dominated by the Witwatersrand Supergroup. The Finsch Diamond Mine (4) is separated from the others and is located west of the Witwatersrand Basin in the Traansval Supergroup Ghaap Dolomite. b) Schematic geological cross section of the Beatrix Gold Mine (www.goldfields.co.za). B2012 was collected near shaft #3. The gold- and uranium rich reef consists of mineralized conglomerates and is less than a meter thick (Fuchs et al., 2017).

collected in Bloemfontein (above ground) and from underground in the mineshafts for comparison. A very limited number of samples for stable noble gases was collected as well.

3. ANALYTICAL METHODS

Separation and purification of krypton and argon from the bulk gas was carried out in laboratories of both the University of Chicago and University of Bern using cryogenic absorption and gas chromatography (Purtschert et al., 2013; Yokochi, 2016). ^{81}Kr/Kr and ^{85}Kr/Kr measurements were performed using the Atom Trap Trace Analysis (ATTA) method (Du et al., 2003; Jiang et al., 2012) at Argonne National Laboratory, USA. Each measurement requires a Kr gas sample of approximately 10 µL STP. ^{39}Ar activities were measured by low-level gas proportional counting in the Deep Laboratory of the Physics Institute, University of Bern, Switzerland (Loosli and Purtschert, 2005; Riedmann and Purtschert, 2016).

Table 1
Results noble gas radionuclides (reference time = sampling time).

Sample location	Type	Code	Sampling Date	Measuring Date	Depth m	^{85}Kr (dpm/cc$_{Kr}$)	^{81}Kr pMKr	^{81}Kr/^{85}Kr (atomic ratio)	Ac$_{max}$ (%)	^{81}Kr^{c} pMKr	^{39}Ar^{c} pMAr
Bloemfontain	Atm air		29.08.2012	05.12.2012		74.0 ± 3.8	96 ± 7				
Bloemfontain	Atm air		09.11.2013	16.05.2014		70.3 ± 1.4	105 ± 7				
Masimong	Mine air		03.09.2012	10.12.2012		68.9 ± 3.5	105 ± 7				
Star Diamond	Mine air		28.08.2012	21.12.2012		71.0 ± 3.6	103 ± 16				
Finsch Air	Mine air		08.11.2013	14.05.2014		70.6 ± 1.4	101 ± 4				
Beatrix 326BH2	GW	B2012	30.08.2012	24.01.2013	1440	4.0 ± 0.5	463 ± 27	3.39	5.8	490	39 ± 9
Beatrix 326BH2	GW	B2012	30.08.2012	21.03.2014	1440	4.7 ± 0.5	485 ± 15	3.04	6.8	510	
Beatrix 326BH2	GW	B2016	01.06.2016	09.02.2017	1440	24.5 ± 0.8	363 ± 11	0.44	35.3	510	
Star Diamond	GW	SD2012	02.09.2012	14.12.2012	640	23.8 ± 2.0	206 ± 16	0.26	34.4	260	
Masimong	GW	M2012	03.09.2012	14.01.2013	1940	10.6 ± 0.8	287 ± 19	0.80	15.4	320	57 ± 8
Finsch BH1	GW	F2013	08.11.2013	12.05.2014	837	1.6 ± 0.4	29 ± 4	0.54	2.3	30	

Ac$_{max}$ Air contamination determined from ^{85}Kr assuming an activity in air of 69.3 ± 1.8 dpm/cc$_{Kr}$ (Eq. (1)); c: contamination corrected values.

For selected stable noble gas analysis, water samples were transferred to copper tubes, which were immediately sealed by pinching the ends. These samples were analysed with a noble gas mass spectrometer at ETH Zürich, Switzerland (Beyerle et al., 2000).

4. RESULTS

4.1. Noble gas radionuclides

The aboveground air samples collected in Bloemfontein and the additional underground air samples collected in the mineshafts (Table 1) exhibited no significant differences with respect to their radio-krypton abundances. ^{81}Kr/Kr ratios agree within uncertainties with the atmospheric value, and all ^{85}Kr measurements are in the range of 69 ± 2 dpm/cc$_{Kr}$ (disintegrations per minute per cm$^3_{STP}$ krypton). This atmospheric ^{85}Kr activity concentration (^{85}Kr$_{atm}$) is in excellent agreement with air samples measured in the southern hemisphere (Australia) during the same period of time (Bollhöfer et al., 2014) and is therefore used to correct for modern air contamination that may have occurred prior to or during sampling. Compared to modern air, the ^{85}Kr activities of the gas samples extracted from the fracture fluids are significantly depleted, in the range of 2–23 dpm/cc$_{Kr}$. Given the antiquity of the groundwater suggested from other studies (Lippmann-Pipke et al., 2011; Lippmann et al., 2003), this variation is presumably caused by atmospheric air contamination during sampling or by contribution from underground production (see below).

Only one sample collected in the Transvaal dolomite (Finsch Mine) showed a depleted ^{81}Kr abundance of 29 pMKr compared to the atmospheric value of 100 pMKr. However, fracture fluids from three mines in the Witwatersrand Supergroup had elevated ^{81}Kr isotopic abundances exceeding 100 pMKr, as high as 460 pMKr for the Beatrix borehole (Table 1). This is in large contrast to the longstanding consensus that subsurface production of ^{81}Kr is negligibly small (Collon et al., 1998; Florkowski, 1992a). This discovery was so unexpected that the possibility of analytical artefacts was investigated by replicating the analyses using newly collected samples. This included a resampling of bulk gas from the Beatrix borehole 326BH2, gas purification with new separation columns, and repeated measurements of ^{85}Kr and ^{81}Kr, all of which confirmed the excess ^{81}Kr in the fracture fluids. A contamination-corrected maximal ^{81}Kr^{c} value is obtained assuming the uncontaminated water was ^{85}Kr-free (Table 1). The corrected ^{81}Kr^{c} value is then:

$$^{81}Kr^{c} = \frac{(\ ^{81}Kr_{m} - \alpha \cdot 100)}{1 - \alpha} \quad (1)$$

with the fraction α of air contamination given by α = ^{85}Kr$_{meas}$/^{85}Kr$_{atm.}$

The ^{39}Ar abundances are expressed as ^{39}Ar/ΣAr ratio relative to the modern atmospheric value (100 pMAr corresponding to ^{39}Ar/ΣAr = 8 × 10^{-16}), where ^{40}Ar constitutes >99% of ΣAr. Fracture waters from Masimong and Beatrix mines had contamination corrected (in analogy to Eq. (1))

Table 2
Stable noble gas concentrations and isotope ratios of the sampled fracture waters compared with concentrations in air saturated water (ASW at 20 °C and 1013 mb).

	$^3He/^4He$	^4He	Ne	Ar	Kr	Xe	C/C_e	C/C_e	$^{40}Ar/^{36}Ar$
		(cm^3_{STP}/g_w)					Ar	Kr	
	(10^{-8})	(10^{-8})	(10^{-7})	(10^{-4})	(10^{-9})	(10^{-9})			
Star Diamond	na	na	na	4 ± 0.6	8.14 ± 0.06	1.35 ± 0.03	0.286	0.120	1324 ± 7
Masimong	4.02 ± 0.86	2832 ± 664	0.005 ± 0.001	0.055 ± 0.02	0.25 ± 0.1	0.05 ± 0.02	0.001	0.004	5486 ± 3170
Beatrix326BH2	4.29 ± 9	na	na	2.72 ± 0.02	8.5 ± 0.08	1.36 ± 0.02	0.079	0.120	3258 ± 22
Finsch	5.29 ± 1	431 ± 22	2.46 ± 0.12	3.46 ± 0.17	70.04 ± 3.5	7.99 ± 0.4	1.108	1.01	296 ± 0.2
ASW	138.4	4.5	1.88		69.8	9.55	1	1	298.6

^{39}Ar abundances of 39 pMAr and 57 pMAr, respectively (Table 1). These depleted $^{39}Ar/\Sigma Ar$ ratios measured here, however, are mainly caused by radiogenic ^{40}Ar enrichment (see below and Table 2). Normalizing to non-radiogenic ^{36}Ar, these data correspond to $^{39}Ar/^{36}Ar$ ratios of 1150 and 430 pMAr, indicating a significant contribution of subsurface-produced ^{39}Ar, as observed elsewhere in high-U concentration rocks (Andrews et al., 1989b; Loosli et al., 1989).

4.2. Stable noble gas results

In the framework of this study, only a limited number of sampling sites and parameters were investigated (Table 2). However, the stable noble gas data of these mines had been reported and thoroughly discussed in three previous studies (Heard et al., 2018; Lippmann-Pipke et al., 2011; Lippmann et al., 2003). Our few results are generally in accordance with previous findings: Helium concentrations showed large excesses compared to air-saturated water (ASW) due to the accumulation of radiogenic He over a very long time period. The $^3He/^4He$ ratios of $4–5 \times 10^{-8}$ are typical for average crustal material and indicate no significant mantle contribution. The fracture water with high ^{81}Kr also showed highly elevated $^{40}Ar/^{36}Ar$ ratios (Table 2) compared to the atmospheric value of 298.6 (Lee et al., 2006) due to the accumulation of radiogenic ^{40}Ar. The range of values up to 5500 agrees with the results of (Lippmann et al., 2003) which reveal $^{40}Ar/^{36}Ar$ ratios between 340 and 11,000. The $^{81}Kr/Kr$ and $^{40}Ar/^{36}Ar$ ratios are correlated, suggesting a lithological origin of ^{81}Kr.

(Lippmann-Pipke et al., 2011) reported excess ^{21}Ne (no data from our campaigns) with neon isotope ratios representing a mixture of air derived neon and a crustal end-member for samples collected in the Masimong and Beatrix mine (Fig. 1 in (Lippmann-Pipke et al., 2011)). Xe isotope ratios for all mines investigated herein clearly indicated a significant contribution of fissiogenic Xe (Fig. 6 in (Lippmann et al., 2003)).

As described by Lippmann et al. (2003), all fracture fluids from mines located in the Witwatersrand Supergroup are strongly depleted in atmospheric Ne, Kr, and Xe due to degassing. This was also confirmed by samples taken in the course of this study (Table 2), and the degassing is most pronounced for the Masimong Mine fracture waters. The water from the Finsch Mine, in contrast, showed noble gas concentrations close to ASW, with higher relative concentrations for the lighter noble gases, pointing to excess air formation during recharge.

In (Heard et al., 2018; Lippmann et al., 2003) it was concluded from the fractionation pattern of the residual noble gas concentrations in the water phase that this gas loss very likely occurred immediately prior to discharge due to the rapid decompression without reaching solubility equilibrium (Aeschbach-Hertig et al., 2008; Lippmann et al., 2003). Our data also provide supporting evidence for this hypothesis. Noble gas depletion factors (Table 2) inversely correlate with the methane content of the water with the highest amount of CH_4 found for the Masimong goldmine (40 cm^3_{STP}/L_W). This methane was probably not present during recharge but has been produced by microbial activities and accumulated in the subsurface over time (Fuchs et al., 2017; Mossman et al., 2008a). However, the case for degassing at an earlier point in time cannot completely be excluded and is discussed below (Section 5.3).

This severe depletion of noble gases from the fluid may accompany kinetic isotope fractionation, the maximum possible degree of which is defined by the mass-dependent diffusivity. The Kr concentration prior to degassing is assumed to be that of air-saturated water at 20 °C and 1013 mbar (Lippmann et al., 2003), and activities of noble gas radionuclides prior to degassing were estimated following the method applied for stable noble gas isotope fractionation (Lippmann et al., 2003). The non-equilibrium degassing could have shifted the isotope ratios of $^{81}Kr/^{83}Kr$ and $^{85}Kr/^{83}Kr$ (the reference isotope for ATTA) by at most ±3.5% for the Masimong sample which showed the highest degree of depletion (Table 2). $^{40}Ar/^{36}Ar$ and $^{39}Ar/^{40}Ar$ ratios are shifted by up to +17% and −6.5% respectively.

5. DISCUSSION

The concentration of the radioactive isotope ^{81}Kr in the fracture groundwater depends on its production rate in surrounding rocks, the water to rock ratio (porosity), the rate of transfer from the rock to the pore space, and radioactive decay (Lehmann et al., 1993). In the discussion below, we re-examine the subsurface production rates and model various release rates so as to identify the primary cause of the elevated ^{81}Kr isotopic abundance in these geological environments.

The production rates of radiokrypton isotopes are primarily determined by the U content of the host rocks, the related subsurface neutron flux (Section 5.1.2) and the

fission yields for ^{81,85}Kr (Section 5.1.1). The flow-path-integrated U content of rocks in contact with the groundwater is not directly measurable due to the heterogeneous distribution of U along the water flow path, but can be estimated using the activity of subsurface-produced ^{36}Cl that is proportional to the U content of host rocks (Section 5.2).

The release rates of produced isotopes from the rock to the water are highly uncertain. Fissiogenic production of ^{81}Kr and ^{85}Kr occurs at the same locations but the two isotopes have very different half-lives. Using ^{85}Kr as a probe, we developed a geochemical model that examines whether the observed data (^{81}Kr/^{85}Kr ratio and ^{85}Kr activity) could result from the previously accepted ^{81}Kr production rate (Section 5.3 and Appendix II). For any rock to groundwater transfer scenario (i.e. continuously or episodic), the geochemical model suggests that the production rate of ^{81}Kr compared to ^{85}Kr needs to be higher than anticipated and sets a conservative limit on the fission yield based on the data (Section 5.4). Taking into account possible secondary processes (Section 5.5) and uncertainties associated with the interpretation (Section 5.6) the implications for groundwater dating under ordinary crustal environment are discussed (Section 5.7).

5.1. Production of ^{81}Kr in the subsurface

5.1.1. Fission reactions

According to present knowledge, 99% of the ^{81}Kr and ^{85}Kr ($T_{1/2} = 10.74$ yr) (Singh and Chen, 2014) in the subsurface is produced by spontaneous fission of ^{238}U (Fabryka-Martin, 1988). A minor production channel for ^{81}Kr and ^{85}Kr is neutron-induced fission of ^{235}U. The cumulative fission yield f_{85} of ^{85}Kr is relatively well known and was determined to be 2.35×10^{-4} with a uncertainty of <10% (Florkowski, 1992a, 1992b; Rozanski and Florkowski, 1978) and (EXFOR 2018 nuclear database; Japan Atomic Energy Agency JENDL). This relatively high yield is caused by the fact that ^{85}Kr is exposed to the isobaric fission-decay chain of mass 85 (Fig. 2). In contrast, ^{81}Kr is protected by the stable ^{81}Br (Collon et al., 1999; Lu et al., 2014). The independent ^{81}Kr fission yield, which is not populated by radioactive decay, is expected to be very small and thus difficult to measure.

Existing theoretical concepts and empirical methods that estimate fission product distributions provide an independent ^{81}Kr spontaneous ^{238}U fission yield f_{81} of $< 10^{-10}$ (Fabryka-Martin, 1988; Florkowski, 1992a; Florkowski et al., 1988; Wahl, 1958). The independent fission yield can be written as a product of three factors (James et al., 1991):

$$f(A,Z,I) = Y(A) \cdot y(A,Z) \cdot R(A,Z,I) \quad (2)$$

where $Y(A)$ is the mass yield, $y(A,Z)$ is the fractional independent yield of all isomers (A,Z) and $R(A,Z,I)$ is the fraction of (A,Z) produced directly as isomer I. $Y(A)$ is known with relatively high accuracy from a large number of experiments and can be described by multimodal Gaussian distributions (James et al., 1991). The

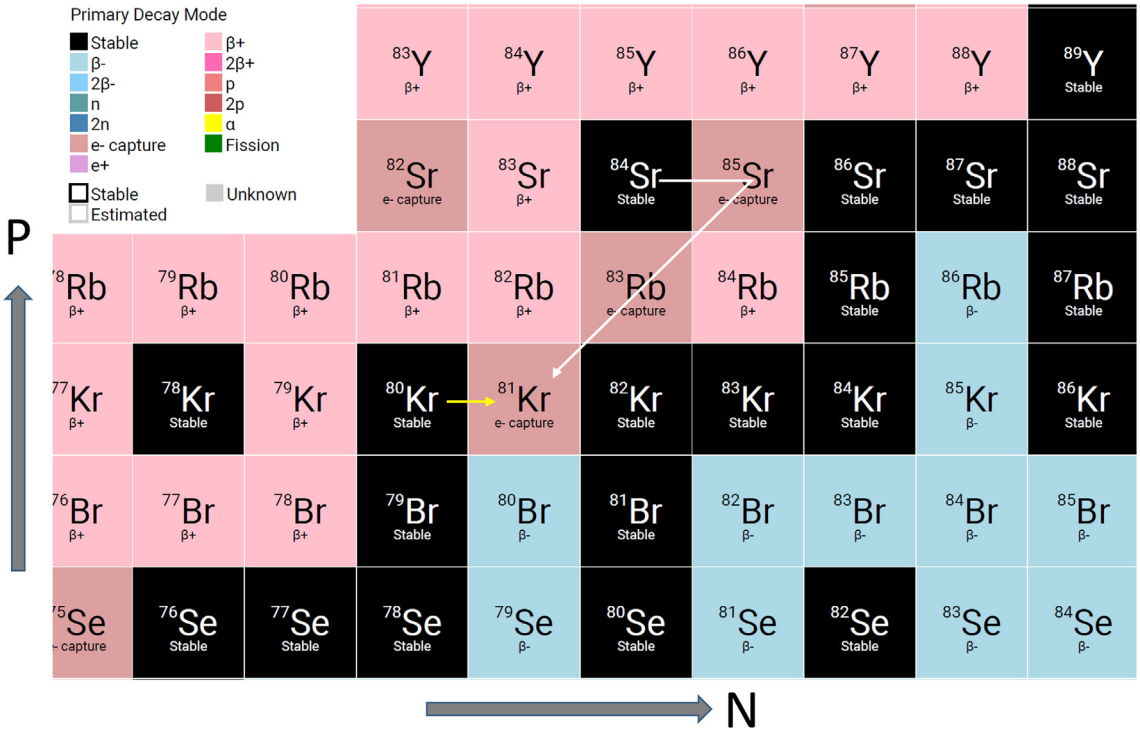

Fig. 2. Nuclide chart showing the position of ^{81}Kr and ^{85}Kr in relation to other stable (black) and radioactive istopes. The stable ^{81}Br shields ^{81}Kr from the neutron-rich β^- decay chain resulting in a much lower cumulative yield from spontaneous ^{238}U fission. Potental other production channels are the ^{84}Sr(n,α)^{81}Kr reaction (indicated by the thin white line) and neutron activiation of the stable ^{80}Kr (yellow arrow). (For interpretation of the references to colour in this figure legend, the reader is referred to the web version of this article.)

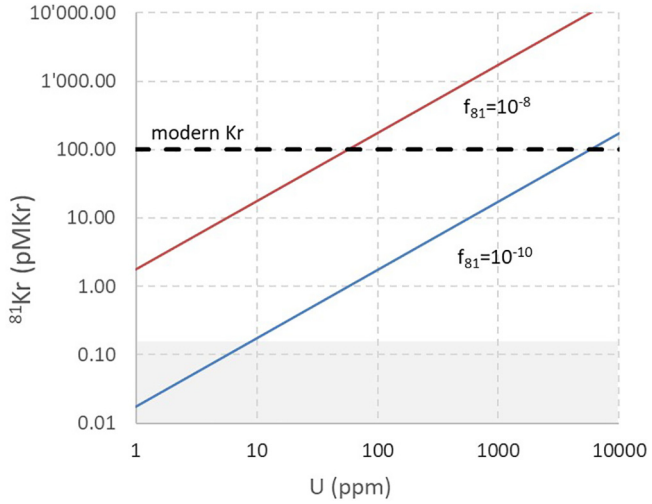

Fig. 3. ^{81}Kr activity in ASW as function of U concentration of the surrounding rock with a porosity of 5% for a complete release of the production-decay equilibrium concentration (Appendix III). The shaded area indicates the current detection limit of the ATTA method. For the commonly accepted but weakly constrained fission yield of $7{\cdot}10^{-11}$ (Florkowski et al., 1988; Lehmann et al., 1993) and average crust composition (U = 2 ppm), underground production is not detectable. A yield of 10^{-8} would result in over modern values for U > 100 ppm in this upper estimate scenario.

charge distribution *y(A,Z)* can be predicted on the basis of the empirical postulate that the charge is equally distributed during the fission reaction and that deviations from the most probable charge Z_p can be described by a symmetrical charge distribution function (Florkowski et al., 1988). Refinements such as the odd-even effect need also to be considered (James et al., 1991). The fractional yield for A = 81 and Z = 36 (^{81}Kr) has never been measured. The yield $f_{81} = 7 \times 10^{-11}$ was estimated based on the fission yield for mass 81 (~0.1%) and the fractional charge yield which is $\sim 7 \times 10^{-8}$ according to the empirical model of (Wahl, 1958).

Provided f_{81}, the resulting ^{81}Kr production-decay equilibrium concentration $Kr_{R,e}$ in a closed-system rock can be calculated as a function of the U concentration. An instantaneous and complete transfer of this pre-accumulated fissiogenic ^{81}Kr from the rock into the pore fluid (with stable Kr content of air-saturated water) provides an upper limit of the fissiogenic ^{81}Kr concentration in the fluid (Appendix III). The resulting ^{81}Kr abundance in the pore water for a porosity 5% as a function of the U concentration is shown in Fig. 3 for two different values of f_{81}. For a $f_{81} < 10^{-10}$, as anticipated by the theoretical estimate above, negligible ^{81}Kr production is expected for typical crustal composition (U ~2 ppm). Only in very U-rich environments with U concentrations >1000 ppm or with much higher than the calculated f_{81}, underground produced fission ^{81}Kr could become significant.

Concentrations of U dissolved in the water are generally <10 ppb for the here investigated mines (Onstott et al., 2006). Fissiogenic production in the water can therefore be neglected.

5.1.2. Neutron-induced reactions

Minor ^{81}Kr production may also occur by neutron-induced reactions. In (Fabryka-Martin, 1988) it was suggested that the reactions ^{80}Kr(n,γ)^{81}Kr on Kr dissolved in water (Paul et al., 2017) and ^{84}Sr(n,α)^{81}Kr on Strontium in rocks and dissolved in water may account for "probably less than 0.1% of the total ^{81}Kr produced" in average crust material. Similar estimates have been made in other studies (Andrews et al., 1991; Lehmann et al., 1993). We have re-evaluated the ^{81}Kr production rates of those two production paths using energy-dependent cross sections from the ENDF data base and a simplified neutron moderation code (Czubek, 1988) that has been previously used in (Yokochi et al., 2012) for the calculation of ^{39}Ar production by the ^{39}K(n,p)^{39}Ar reaction. 90% of neutrons in the deep lithosphere (neglecting cosmogenic production) originate from (α,n) reactions on light elements with α particles produced in radioactive decays of naturally occurring ^{232}Th; ^{235}U, and ^{238}U. The remaining 10% of subsurface neutrons originate directly from spontaneous fission (Šrámek et al., 2017). The resulting primary (α,n) and fission yield neutron spectra show a peak in the 1–2 MeV range (Šrámek et al., 2017). The production-relevant secondary neutron spectra in the rock result from neutron scattering and absorption reactions and depend therefore on the bulk rock composition (Feige et al., 1968; Leya and Wieler, 1999; Yatsevich and Honda, 1997). With reaction cross sections taken from ENDF database (shown in Fig. 2, Appendix I) and a moderated secondary neutron spectrum for average continental crust composition (Czubek, 1988; Šrámek et al., 2017; Yokochi et al., 2012), the production rate ^{i}P (in a/cm$^{-3}_{rock}$ s^{-1}) of isotope *i* is calculated as:

$$P = [C_i] \cdot \int_E \phi(E) \cdot \sigma_i(E) dE \qquad (3)$$

with target nuclide concentration $[C_i]$ (a cm^{-3}), moderated neutron flux ϕ(E) (n cm^{-2}s^{-1}) and reaction cross section σ_i(E) (barn).

Table 3
U, Th and K concentration in rock samples collected in the Beatrix goldmine.

Formation	Rock type	U (ppm)	Th (ppm)	K (%)
Beatrix Reef, average[a]	conglomerate	1130	81.2	0.6
Beatrix average[a]	quartzite	74	7.3	1.3
Beatrix, selected hanging & foot	quartzite	4.7	31.2	1.3
Beatrix, quartzite[a]	quartzite	3	2.7	1.7
Beatix, quarzite	quartzite	1	2.6	0.4
Beatix, quarzite	quartzite	4.5	11.6	0.7

[a] From Lippmann et al. (2003).

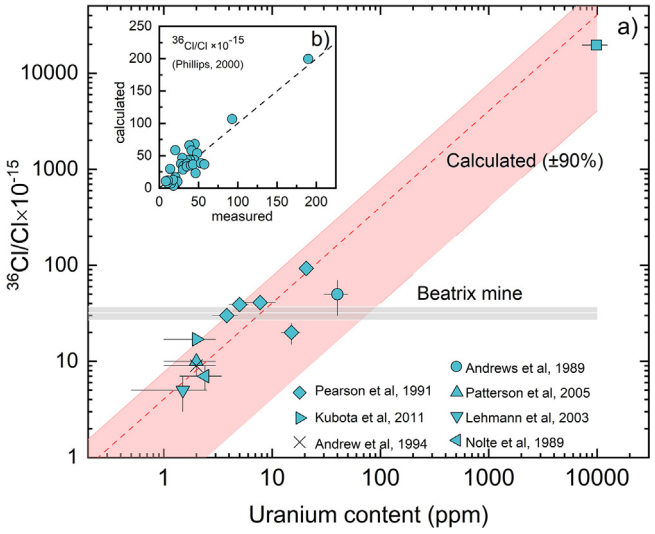

Fig. 4. a) Calculated ^{36}Cl/Cl secular equilibrium ratios as a function of the U concentration of the surrounding rock formation (Eq. (2), assuming granitic rock composition and U/Th = 10). Also shown are data from different case studies. The grey bar indicates the average ^{36}Cl/Cl ratio of 6 samples from the Beatrix Gold Mine (Lippmann et al., 2003), where the highest ^{81}Kr enrichment was observed. Assuming secular equilibrium these samples indicates an average U content of < 100 ppm. b) Comparison of calculated and measured equilibrium subsurface ^{36}Cl/Cl ratios from 36 samples taken in various aquifers (Phillips, 2000).

The target density of ^{80}Kr is estimated based on krypton dissolved in ASW (20 °C and 1013 mb) in a water-filled rock porosity of 5%. Strontium concentrations in the rocks of Witwatersrand Supergroup range up to 200 ppm (Wronkiewicz and Condie, 1987). In the groundwater values between 0.3 and 6.4 mg/L were measured for our sampling locations (Table 3 Appendix I). As a reference and for neutron flux verification purposes, also the production rate of ^{39}Ar was calculated (for 2.5% K). All production rates were normalised to a U concentration of 1 ppm and a Th/U ratio of 10 (details about the production calculations can be found in Appendix I where Table 1 lists the main results in comparison with the fissiogenic ^{81}Kr production assuming a cumulative yield of 10^{-10}). In summary the neutron activation reactions ^{84}Sr(n,α)^{81}Kr in the rock and the water and ^{80}Kr(n,γ)^{81}Kr in the water contribute in total less than 2% of the fissiogenic ^{81}Kr production rate. The spontaneous ^{238}U fission is the dominant ^{81}Kr production channel under ordinary crustal environment, in agreement with previous estimates. The ^{39}Ar production rate on the other side, is about 11 orders of magnitude higher compared to the ^{81}Kr production for typical crust composition (Šrámek et al., 2017).

Based on these conclusions, only fission production is considered in the following discussion of the ^{81}Kr data with regard to different production -release scenarios in the rock.

5.2. ^{36}Cl and ^{39}Ar as proxy of the integrated U content along the water flow path

The U, Th, and K contents of rock samples of the Witwatersrand Supergroup collected from the Beatrix Gold Mine vary significantly among lithologies (Table 3). U ranges up to 12 ppm U in quartzite, but can be as high as 1000 ppm in the gold-bearing formations (“reefs”). The estimation of a representative U content that is integrated over time and space throughout the fluid flow path is not trivial (Lippmann et al., 2003), but may be constrained based on the ^{36}Cl activity of dissolved chloride. In the subsurface, ^{36}Cl is produced by the reaction ^{35}Cl(n,γ)^{36}Cl with thermal neutrons originating from U and Th fission and from (α, n) reactions on light elements of the rock matrix (Feige et al., 1968; Lehmann and Purtschert, 1997). With a half-life of 301 kyr, ^{36}Cl is a neutron flux (thus U content) monitor that integrates over similar timescales as ^{81}Kr, assuming no recent change in Cl content. The comparison

of calculated and measured equilibrium subsurface nucleogenic ^{36}Cl/Cl ratios (Fig. 4b) reveals generally good agreement (Cornett et al., 1996; Phillips, 2000). The relationship between the secular equilibrium ^{36}Cl/Cl ratio R_{eq} and the U and Th concentrations can simply be described by (Andrews et al., 1989a; Balderer and Synal, 2004):

$$R_{eq} = (\alpha \cdot [U] + \beta \cdot [Th]) \cdot 10^{-15} \quad (4)$$

with formation specific parameters α and β (Balderer and Synal, 2004; Pearson Jr. et al., 1991) and U and Th concentrations given in ppm. This relationship, which was determined based on Eq. (3), is plotted for granitic rock ($\alpha = 0.86$, $\beta = 0.3$, U/Th = 10) in Fig. 4 a) and compared with measurements from several field studies including those from a U mine. Typical crust material with ~2 ppm U results in equilibrium ratios of 5–15 × 10^{-15} (Lehmann et al., 2003; Love et al., 2000; Phillips et al., 1986; Sturchio et al., 2004). In high U formations values over 10,000 × 10^{-15} have been observed (Balderer and Synal, 2004; Cornett et al., 1996). ^{36}Cl/Cl ratios only reflect an effective U content integrated along the water flow path if no Cl from formations low in U was dissolved after the fracture waters percolated the U-rich formations. In this case the integrated U content would be underestimated. However, such a recent Cl addition would result in decreasing ^{36}Cl/Cl ratios with increasing Cl content – contrary to what was observed (Lippmann et al., 2003). The average ^{36}Cl/Cl ratio in fracture waters from the Beatrix Gold Mine, where the ^{81}Kr enrichment was highest, was $32 \pm 5 \times 10^{-15}$ (mean of 6 measurements Table 5: (Lippmann et al., 2003), suggesting an effective U concentration of the rock ranging from approximately 3 to 100 ppm (Fig. 4a).

Supporting evidence can be derived from our ^{39}Ar data. The ^{39}Ar production rate in a rock with 100 ppm U is ~1000 atoms/kg$_{rock}$/yr (Table 1, Appendix I). Assuming production-decay equilibrium in the rock, a porosity of 5% and a release factor of 1% a maximal ^{39}Ar concentration in the groundwater of 194 a/cm$^3_{water}$ is estimated. In ASW this translates to a ^{39}Ar/∑Ar ratio of 2.34 × 10^{-14} or 2900 pMAr (neglecting ^{39}Ar produced on K dissolved in the water, which could be of similar order of magnitudes). This is already higher than the observed ^{39}Ar/^{36}Ar enrichment of 1120 pMAr (Table 1). Thus, the ^{39}Ar data also suggest an U concentration of likely not more than 100 ppm (for rocks in contact with the groundwater over the last approximately 800 years of residence: 3 × $T_{1/2}$ (^{39}Ar)).

In conclusion, we estimate an upper limit of 100 ppm U for rocks hosting the water-conductive fractures with ^{81}Kr abundances of >100 pMKr (Beatrix and Masimong gold mines and Star diamond mine). A 0.4 ppm U concentration is assumed for the Finsch Diamond Mine which is hosted by the Transvaal Supergroup Ghaap dolomites (Munro, 2013; Nicolaysen et al., 1981).

5.3. Production and transfer of fissiogenic ^{85}Kr and ^{81}Kr from rocks to fluids

The radioactive isotopes ^{81}Kr and ^{85}Kr are produced underground at rates ^{81}P and ^{85}P ($^{85,81}P = {}^{238}U \times \lambda_{SF} \times f_{85,81}$) with spontaneous fission decay constant $\lambda_{SF} = 8.56 \times 10^{-17} yr^{-1}$) and fission yields $f_{85,81}$ for ^{85}Kr and ^{81}Kr, respectively, and may be released from the rock into the fluid in contact. The behaviour of this isotope transfer can be modelled as a first order rate process to cover a wide range of transfer rates (See Appendix II for details). The isotope concentration [atoms/cc$_{rock}$] in the rock matrix ($\equiv {}^{85}Kr_R$) is expressed as (Yokochi et al., 2012):

$$\frac{d\ {}^{85}Kr_R}{dt} = {}^{85}P - (\lambda_{85} + \alpha)\ {}^{85}Kr_R \quad (5)$$

where α and λ_{85} are the loss rate and the decay constant, respectively (note: the loss rates for ^{85}Kr and ^{81}Kr are assumed to be identical in the following as they originate from the same production site within the rock matrix: $\alpha_{81} = \alpha_{85} = \alpha$). The ^{85}Kr concentration in the groundwater ($\equiv {}^{85}Kr_W$) to which the isotope is released is then given by:

$$\frac{d\ {}^{85}Kr_W}{dt} = \frac{\alpha}{\phi}\ {}^{85}Kr_R(t) - \lambda_{85}\ {}^{85}Kr_W(t) \quad (6)$$

where the porosity ϕ is assumed to be small (≪1). The bulk porosity of the Witwatersrand Supergroup quartzite is approximately 0.5–1% (Silver et al., 2012). It is worthwhile to note here, that porosity in this model is not necessarily the physical volume ratio of water to rock, but to the rock volume that effectively contributes radioisotope to the water. Solving Eq. (6) leads to the following temporal evolution in the water phase:

$$Kr_W(t) = \frac{{}^{85}P}{\lambda_{85} \cdot \phi} \cdot \frac{\alpha}{\alpha + \lambda_{85}} \cdot (1 - \exp(-(\alpha + \lambda_{85}) \cdot t)) \quad (7)$$

The rock was assumed to have started to lose Kr at t = 0, hence the $^{85}Kr_R$ concentration of the rock was in production-decay equilibrium ($= {}^{85}P/\lambda_{85}$), which provides an upper limit (see Appendix II for detail). The initial concentration in the water $^{85}Kr_W$ was set as 0. The system will approach a steady state isotope concentration given by $^{85}P \times \alpha/[\phi \times \lambda_{85} \times (\alpha + \lambda_{85})]$ with a time constant of $\alpha + \lambda_{85}$.

Following the same approach for ^{81}Kr, the ^{81}Kr/^{85}Kr ratio can be expressed as a function of release rate α and time t since the release started:

$$\left(\frac{{}^{81}Kr}{{}^{85}Kr}\right)_W(t) = \frac{{}^{81}P}{{}^{85}P} \cdot \frac{\lambda_{85}(\lambda_{85} + \alpha)}{\lambda_{81}(\lambda_{81} + \alpha)} \cdot \frac{1 - \exp(-(\lambda_{81} + \alpha) \cdot t)}{1 - \exp(-(\lambda_{85} + \alpha) \cdot t)} \quad (8)$$

The concentration ratio ^{81}Kr/^{85}Kr in the fluid will initially inherit that of the rock in production-decay-loss equilibrium, $[{}^{81}P/(\lambda_{81} + \alpha)]/[{}^{85}P/(\lambda_{85} + \alpha)]$, then increases with time due to slower ^{81}Kr ingrowth by a factor of $(\lambda_{85} + \alpha)/(\lambda_{81} + \alpha)$. Since ^{85}Kr and ^{81}Kr are both produced by fission of U, the ratio of the production rate (^{81}P/^{85}P) does not require knowledge of the U content of the rock: $^{81}P/{}^{85}P = {}^{238}U \times \lambda_{SF} \times f_{81}/({}^{238}U \times \lambda_{SF} \times f_{85}) = f_{81}/f_{85}$.

An upper limit (UL) of the ^{81}Kr/^{85}Kr ratio in the fluid, corresponds to the steady-state composition at t → ∞ which depends on α. This ratio normalized to the respective

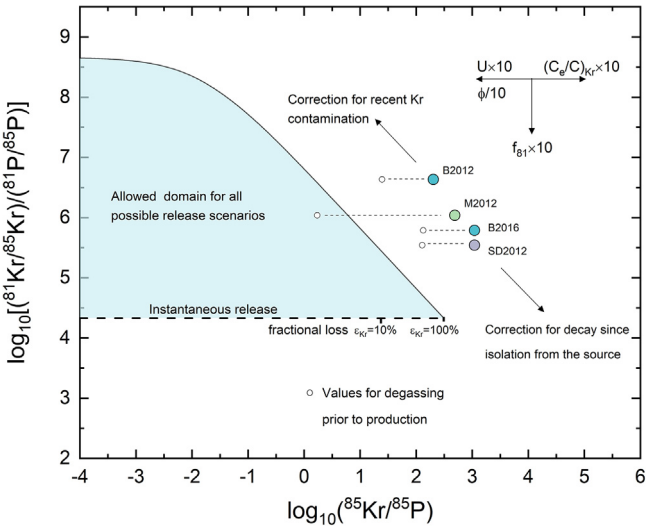

Fig. 5. Anticipated range of (^{81}Kr/^{85}Kr)/(^{81}P/^{85}P) ratio for given ^{85}Kr contents and production rates. The blue area indicates the allowed model domain (see text). Small open circles represent actual data for a ^{81}Kr fission yield f_{81} of 10^{-10} and a U concentration of 100 ppm. If degassing has occurred after production, the values are shifted to the right according to the degrees of degassing (filled circles). Also shown are the effects of air contamination during sampling and ^{85}Kr decay due to a delay time from the site of production to the sampling point. Higher than anticipated U concentrations and a lower porosity would shift the data points to the left (by one unit for a factor of 10 change). To achieve consistency between the degassing corrected data and the allowed model domain a ^{81}Kr fission yield of 1×10^{-8} or an U concentration of 10,000 ppm has to be assumed (or a combination of both). (For interpretation of the references to colour in this figure legend, the reader is referred to the web version of this article.)

fission yields can be expressed as a function of $^{85}Kr_W$ using α as a parametric variable:

$$\frac{(\frac{^{81}Kr}{^{85}Kr})_{W,UL}}{\frac{f_{81}}{f_{85}}} = (\phi \cdot \lambda_{81} \cdot (1 - \frac{\lambda_{81}}{\lambda_{85}}) \cdot \frac{^{85}Kr_W}{^{85}P} + (\frac{\lambda_{81}}{\lambda_{85}})^{2})^{-1} \quad (9)$$

Note that this upper limit line covers the entire range of release rates α, from practically episodic loss at $\alpha \geq 1$ to slow continuous loss at $\alpha \sim 0$. The lower limit of our model domain is defined by the production-decay equilibrium, $[^{81}P/\lambda_{81}]/[^{85}P/\lambda_{85}]$, which is e.g. realized for a rapid release from a previously closed rock. These two constraints define a possible range of $(^{81}Kr/^{85}Kr)_W/(f_{81}/f_{85})$ values for a given $^{85}Kr_W/^{85}P$ as shown in Fig. 5. The possible range of the unknown f_{81}/f_{85} (thus f_{81}) can therefore be estimated based on the measured $^{85}Kr_W$, $(^{81}Kr/^{85}Kr)_W$ and the U content of the rock which defines ^{85}P.

5.4. Constraining the ^{81}Kr fission yield

The waters have experienced partial gas loss and possibly mixing with the gas trapped in the fracture cavity created by dewatering shortly before or during sampling. These processes need to be taken into account. We estimate a possible range of the ^{81}Kr fission yield f_{81} by considering processes that potentially affect the $(^{81}Kr/^{85}Kr)_W$ ratio and the $^{85}Kr_W$ concentration in the fracture water. Recent krypton ($^{85}Kr_{rc}$), regardless of whether it is due to mixing of young groundwater or due to modern air contamination during sampling, will increase the ^{85}Kr isotopic abundance and decrease the $^{81}Kr/^{85}Kr$ ratio. Without correction, the subsurface-produced ^{85}Kr would be overestimated. With a fraction f (=0 to 1) of $^{85}Kr_{rc}$ to the observed $^{85}Kr_{ob}$, it follows:

$$^{85}Kr_{corr} = {}^{85}Kr_{ob} \cdot (1 - f) \quad (10)$$

$$(\frac{^{81}Kr}{^{85}Kr})_{corr} = \frac{^{81}Kr_{ob} - (\,{}^{85}Kr_{ob} \cdot f \cdot (\frac{^{81}Kr}{^{85}Kr})_{rc})}{^{85}Kr_{ob} \cdot (1 - f)} \quad (11)$$

The modern (2012) atmospheric $(^{81}Kr/^{85}Kr)_{rc}$ ratio was used to deduce the maximum possible degree of correction. The resulting corrected $^{85}Kr_{corr}$ is lower than the observed $^{85}Kr_{ob}$ values and the corrected $(^{81}Kr/^{85}Kr)_{corr}$ ratio is higher for $f \neq 0$ (Fig. 5).

A delay between sites of highest production to the sampling point will increase the $^{81}Kr/^{85}Kr$ ratio due to the shorter half-live of ^{85}Kr. This is considered by a reversed decay correction:

$$^{85}Kr_d = {}^{85}Kr_{ob} \cdot \exp(\lambda_{85} \cdot t) \quad (12)$$

$$(\frac{^{81}Kr}{^{85}Kr})_d = (\frac{^{81}Kr}{^{85}Kr})_{ob} \cdot \exp((\lambda_{81} - \lambda_{85}) \cdot t) \quad (13)$$

which shifts the corrected values toward the lower right corner in Fig. 5. Degassing at any point in time will only marginally affect the $^{81}Kr/^{85}Kr$ ratio. If degassing happened prior to the production no fissiogenic ^{85}Kr would be lost and the observed isotopic abundances can directly be interpreted (open circles in Fig. 5). However, as already discussed in Section 4.2, a late degassing scenario (after production) seems more likely because the fractionation pattern of the dissolved noble gases points to rapid degassing in non-equilibrium and gas stripping due to methane oversaturation (Lippmann et al., 2003; Slater et al., 2006). Such degassing may have occurred during sampling but one will also expect degassing to occur before sampling in the formation around the mineshafts because of dewatering as a result of mining activities.

The Kr depletion factor ($\equiv C/C_e$) compared to ASW at 20 °C and a recharge elevation of 1750 m (Lippmann et al., 2003) of our samples ranges from 0.004 for the Masimong mine to 0.12 for the Beatrix mine (Table 2). The ^{85}Kr concentrations prior to degassing were estimated following Lippmann et al. (2003) and are shown as filled circles in Fig. 5.

Whether or not our data fall within the permissible zone (between the upper limit defined by Eq. (9) and the lower limit at $[^{81}P/\lambda_{81}]/[^{85}P/\lambda_{85}]$) depends on the U content (controlling ^{85}P), the porosity (governing $^{85}Kr_w$) and the fission yield of ^{81}Kr. The relevant porosity here is the ratio of the fluid filled volume to the volume of the rock that contributes to production. This ratio is likely larger than the matrix porosity of the quartzite of 1% (Silver et al., 2012) which describes the porosity of an intact piece of rock without fractures. In the following, a porosity of 5% is assumed. According to the previous section, an upper limit U content of 100 ppm was estimated for the Witwatersrand formations (Beatrix, Masimong and Star Diamond). With a ^{81}Kr fission yield of 10^{-10} our data corrected for gas loss (filled circles in Fig. 5) plot outside the allowed model domain. It indicates that the observed data cannot be explained regardless of release rates (α), delay time or degree of air contamination, which shifts the data parallel to the upper model boundary (as it is the case for the two samples taken in different years at the Beatrix borehole). To create consistency between the data and the model either the porosity needs to be lowered or the effective U content needs to be increased by two orders of magnitude (arrows in Fig. 5). Both options are implausible. We conclude a higher than previously assumed fission yield f_{81} (which moves our data points downwards in Fig. 5). If our U and porosity estimates are accurate a fission yield f_{81} of $\sim 1 \times 10^{-8}$ is concluded. The data uncorrected for the gas loss are encompassing the unlikely case of degassing prior to fissiogenic ^{85}Kr accumulation (open circles in Fig. 5), all data except the one from the Masimong gold mine would still require higher than previously anticipated f_{81}.

Relatively conservative enhancements of fission yield over the previous estimates are obtained for relatively high Kr release rate, slower rock-to-fluid transfer would require even a higher fission yield. Heavy noble gases (i.e. all but He) are well contained in most crustal rocks at inter and intra granular sites (Ballentine and Burnard, 2002). However if U is concentrated on the mineral or fracture surface a more effective release is expected. This possibility is discussed in the following two sections.

5.5. Special case for instantaneous release

The general model presented above provides a fission yield f_{81} for a variety of parameters and processes but still depends on the assumed U content of the rocks. If the measured ^{81}Kr/^{85}Kr ratio represent that of the fluid in contact with the subsurface production site (i.e. no atmospheric radiokrypton nor delay since isolation from the source), the ^{81}Kr fission yield can be estimated solely from this ratio provided a rapid release ($\alpha \gg \lambda_{85}$). In our model, it is represented by the lower bound of the allowed model domain (see Fig. 5). The ^{81}Kr/^{85}Kr ratio of the fluid is defined by the production-decay equilibrium ratio and thus the fission yield ratio:

$$\left(\frac{^{81}Kr}{^{85}Kr}\right)_{meas} = \frac{P_{81}\cdot\lambda_{85}}{P_{85}\cdot\lambda_{81}} = \frac{f_{81}}{f_{85}}\cdot\frac{\lambda_{85}}{\lambda_{81}} \quad (14)$$

This means that the fission yield f_{81} can directly be calculated from the measured ^{81}Kr/^{85}Kr ratio without any assumption about the U concentration in the rock.

$$f_{81} = f_{85}\cdot\left(\frac{^{81}Kr}{^{85}Kr}\right)_{meas}\cdot\frac{\lambda_{81}}{\lambda_{85}} \quad (15)$$

Best sampling conditions with minimal air contamination were realized for sample B2012 (Table 1). With an ^{81}Kr/^{85}Kr ratio of 3.2 for the B2012 sample (mean of 2 measurements (Table 1)) and using Eq. (14), a ^{81}Kr fission yield of 3.5×10^{-8} is calculated, for which case the B2012 data point falls onto the right corner of the allowed area in Fig. 5. This provides additional evidence for the correctness of the assumed U content because this represents indeed the situation for 100% fractional release of ^{85}Kr (and ^{81}Kr) as postulated in this fast release scenario (Appendix III).

5.6. Conceptual uncertainties

The least constrained parameter in our model is the time-integrated U content of the rocks from which ^{81}Kr and ^{85}Kr are released along the water flow path. Three proxies were considered: measured U concentrations in bulk rocks (this study, Lippmann et al., 2003, 2011) and U concentrations derived from ^{36}Cl and ^{39}Ar data, which both agreed on an upper estimate of 100 ppm (Beatrix average Table 3). If this does not represent the mean U contents of the host rock from which ^{81}Kr was released to the fracture water, then the fission yield estimates need to be corrected accordingly. A recent textural study of material from the carbon leader reef (Fuchs et al., 2017) reported aggregates of nanometre-size uraninite particles in pore spaces, creating a large surface/volume ratio that facilitates the release and the mobility of U fission products. Geochemical studies show a correlation between carbon, gold and uranium concentrations in the rocks of the Witwatersrand Basin suggesting a genetic association to hydrothermal processes (Fuchs et al., 2017; Mossman et al., 2008; Rodney et al., 2016). If the sampled fracture water interacted with U and gold rich reef layers a higher effective U content (>20,000 ppm) would plot our data points to the left towards the allowed model domain in Fig. 5. Although a potential effect of such high U content in rocks cannot be completely excluded, it would in turn be enigmatic why this is not reflected by an elevated ^{36}Cl or ^{39}Ar content of dissolved Cl. Finally, a much lower porosity than the anticipated 5% is another possible factor that could contribute to enhanced radiokrypton concentrations in the fracture waters.

5.7. Significance of underground production for ^{81}Kr groundwater dating

With a fission yield f_{81} ($\sim 10^{-8}$) that is up to two orders of magnitude higher than previously assumed the significance of ^{81}Kr underground production for groundwater

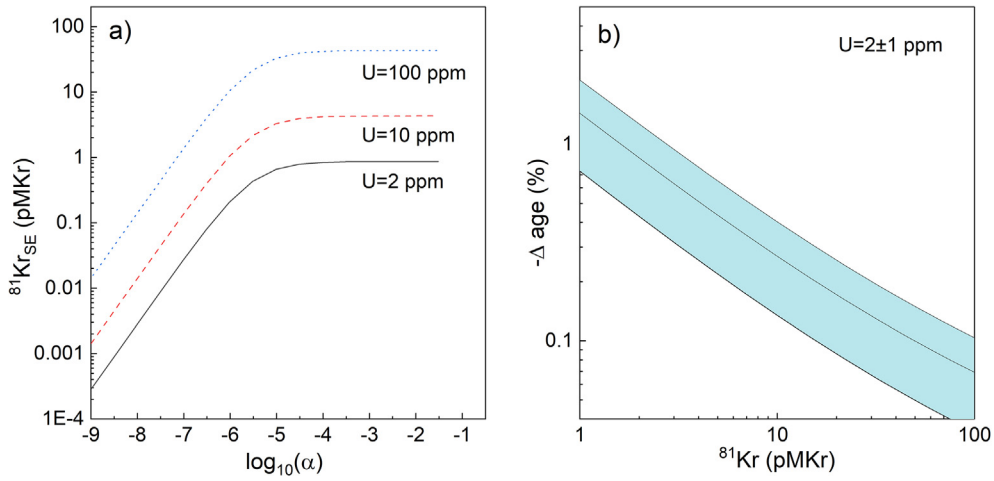

Fig. 6. Effect of underground production in rocks with porosity of 20% for a fission yield of 1×10^{-8}: a) Secular equilibrium (SE) ^{81}Kr activity in groundwater as a function of the release rate α. b) Deviation of groundwater age due to underground production as a function of the measured ^{81}Kr abundance for average crustal composition (U = 2 ± 1 ppm) and a ^{81}Kr release rate $\alpha = 3.4 \cdot 10^{-7}$ yr^{-1}.

dating needs a revaluation. Fig. 3 shows the respective secular equilibrium ^{81}Kr isotopic abundance in groundwater for a release rate $\alpha \gg \lambda_{81}$ where all produced ^{81}Kr atoms are transferred to the fluid prior to decay (Appendix III). This upper (and unlikely) estimate results in a measurable secular equilibrium concentration in low porosity aquifers (<5% e.g. in fractured rocks) and typical crustal U concentrations. However, in most porous media aquifers lower secular equilibrium concentrations can be expected because of higher porosities of ~20%. Finally, the secular equilibrium ^{81}Kr activity in the groundwater depends on the release rate α (Fig. 6a) that is difficult to assess. For a release rate of 3.4 10^{-7} yr^{-1}, which corresponds to a fractional loss coefficient of 10% (Appendix III) the deviation of ages due to underground production can be calculated as a function of the measured ^{81}Kr abundances (Fig. 6b). The age underestimation is <1% for ^{81}Kr values >10 pMKr and approximately 1–4% at the current ^{81}Kr detection limit of 1 pMKr (or age of 1.5 Myr). The sample from the Finsch Diamond Mine (Table 1) collected in the Transvaal Supergroup Ghaap dolomite with an average U concentrations of 0.4 ppm (Nicolaysen et al., 1981) revealed a ^{81}Kr value of 27 ± 4 pMKr after correction for air contamination. The resulting decay age is 432 ± 60 kyr. The consideration of underground production with above listed assumptions results in an age correction of +1 kyr, far below the error caused by analytical uncertainty.

6. CONCLUSIONS

For the first time, underground production of ^{81}Kr was detected in groundwater. The observed ^{81}Kr/Kr ratios exceed the atmospheric level by a factor of up to 5, which makes decay dating impossible in this case, contrary to other studies of very old groundwater (Gerber et al., 2017; Matsumoto et al., 2018; Sturchio et al., 2014; Yechieli et al., 2019; Yokochi et al., 2019). Isotope fractionation processes or degassing cannot explain these anomalies. The elevated ^{81}Kr values observed are caused by the high U concentrations in low porosity fractured rock formations of the Welkom gold fields (Dwyer, 1993) but likely also by a higher production rate than previously assumed. We developed a model that describes production and release of the radionuclides ^{85}Kr and ^{81}Kr and takes into account various water-rock isotope transfer rates, contribution of young atmospheric radiokrypton isotopes, as well as timing of production-release along the flow path of the fracture waters. The U content of the rock in contact with the groundwater was estimated based on bulk rock analyses and ^{36}Cl/Cl ratios of dissolved chloride which indicate consistently an effective U content of the rock of at most 100 ppm. With this estimate, our data are in contradiction with previously estimated fission yields of ^{81}Kr of $<10^{-10}$ for spontaneous fission of ^{238}U but rather indicate either a fission yield significantly higher than the current estimate or alternative production reactions yet to be considered. This presents a rare case where a geological analogy constrains physical constants owing to the long integration time scale.

More studies will be necessary in order to further constrain the production channels for ^{81}Kr in the subsurface. This study was carried out in an "extreme" hydrological environment within the world's greatest deposit of gold and uranium. In aquifers with typical crustal composition, the effect of underground production is negligible given the current analytical precision and other processes that affect the interpretation of dating tracers in terms of groundwater residence times, even considering potentially higher fission yields. Caution needs to be taken in U-rich and low porosity formations and where simultaneously ^{36}Cl/Cl ratios above 20×10^{-15} and ^{40}Ar/^{36}Ar ratios significantly above the atmospheric value are detected.

Declaration of Competing Interest

The authors declare that they have no known competing financial interests or personal relationships that could have appeared to influence the work reported in this paper.

ACKNOWLEDGEMENTS

This project was funded by the U.S. National Science Foundation, Grant number 1141435, to TLK, and by the Department of Energy, Office of Nuclear Physics, under contract DE-AC02-06CH11357. We also thank the Swiss Science Foundation for financial support (Grant number 200020_172550). We are grateful to Thomas Rauscher for providing scientific inputs on theoretical aspect of subsurface radionuclide production. Z.-T. L. and W. J. are supported by the National Key Research and Development Program of China (2016YFA0302200) and the Chinese Academy of Sciences (XDB21010200). We thank the management and workers of Sibanya-Stillwater and Beatrix Gold Mine, of Petra Diamonds and Finsch Diamond Mine, of Frontiers Diamonds and Star Diamond Mine and of Harmony Gold Mining and Masimong Gold Mine for providing access to the mines and assistance in sampling.

APPENDIX A. SUPPLEMENTARY MATERIAL

Supplementary data to this article can be found online at https://doi.org/10.1016/j.gca.2020.11.024.

REFERENCES

Aeschbach-Hertig W., El-Gamal H., Wieser M. and Palcsu L. (2008) Modeling excess air and degassing in groundwater by equilibrium partitioning with a gas phase. *Water Resour. Res.* **44**.

Agency I. A. E. (2013) Isotope Methods for Dating Old Groundwater. International Atomic Energy Agency, Vienna.

Aggarwal P. K., Fröhlich K., Glynn P. D., Phillips F. M., Plummer L. N., Purtschert R., Reilly T. E., Sanford W., Sturchio N. C., Stute M., Suckow A., Torgersen T. and Yokochi R. (2013) Isotope Methods for Dating Old Groundwater. International Atomic Energy Agency, Vienna.

Aggarwal P. K., Matsumoto T., Sturchio N. C., Chang H. K., Gastmans D., Araguas-Araguas L. J., Jiang W., Lu Z.-T., Mueller P., Yokochi R., Purtschert R. and Torgersen T. (2015) Continental degassing of ^{4}He by surficial discharge of deep groundwater. *Nat. Geosci.* **8**, 35–39.

Andrews J. N., Davis S. N., Fabryka-Martin J., Fontes J.-C., Lehmann B. E., Loosli H. H., Michelot J.-L., Moser H., Smith B. and Wolf M. (1989a) The in situ production of radioisotopes in rock matrices with particular reference to the Stripa granite. *Geochim. Cosmochim. Acta* **53**, 1803–1815.

Andrews J. N., Florkowski T., Lehmann B. E. and Loosli H. H. (1991) Underground production of radionuclides in the Milk River aquifer, Alberta, Canada. *Appl. Geochem.* **6**, 425–434.

Andrews J. N., Hussain N. and Youngman M. J. (1989b) Atmospheric and radiogenic gases in groundwaters from the Stripa granite. *Geochim. Cosmochim. Acta* **53**, 1831–1841.

Balderer W. and Synal H. A. (2004) Tracing groundwater from uranium rich environments by ^{36}Cl isotope method: possibilities for natural analogue studies. *Nucl. Instrum. Methods Phys. Res., Sect. B* **223–224**, 471–478.

Ballentine C. J. and Burnard P. G. (2002) Production, release and transport of noble gases in the continental crust. In *Noble Gases in Cosmochemistry and Geochemistry* (eds. D. Porcelli, C. Ballentine and R. Wieler). Mineralogical Society of America, Geochemical Society.

Beyerle U., Aeschbach-Hertig W., Imboden D. M., Baur H., Graf T. and Kipfer R. (2000) A mass spectrometric system for the analysis of noble gases and tritium from water samples. *Environ. Sci. Technol.* **34**, 2042–2050.

Bollhöfer A., Schlosser C., Ross J. O., Sartorius H. and Schmid S. (2014) Variability of atmospheric krypton-85 activity concentrations observed close to the ITCZ in the southern hemisphere. *J. Environ. Radioact.* **127**, 111–118.

Collon P., Cole D., Davids B., Fauerbach M., Harkewicz R., Kutschera W., Morrissey D. J., Pardo R., Paul R., Sherrill B. M. and Steiner M. (1999) Measurement of the long-lived radionuclide ^{81}Kr in pre-nuclear and present-day atmospheric krypton. *Geochim. Cosmochim. Acta* **85**, 13–19.

Collon P., Kutschera W., Davids B., Fauerbach M., Harkewics R., Morrissey D., Sherrill B., Steiner M., Lehmann B. E., Loosli H. H. and Purtschert R. (1998) First Attempt at Dating Groundwater from the Great Artesian Basin of Australia with ^{81}Kr using AMS, ICOG-9. Chinese Science Bulletin, Chinese Academy of Science, Beijing, p. 27.

Cornett R. J., Cramer J., Andrews H. R., Chant L. A., Davies W., Greiner B. F., Imahori Y., Koslowsky V., McKay J., Milton G. M. and Milton J. C. D. (1996) In situ production of ^{36}Cl in uranium ore: A hydrogeological assessment tool. *Water Resour. Res.* **32**, 1511–1518.

Czubek J. A. (1988) SLOWN2.BAS Program for Calculation of the Rock Neutron Slowing Down Parameters. Institute of Nuclear Physics, Cracow.

Dong X.-Z., Ritterbusch F., Chu Y.-Q., Gu J.-Q., Hu S.-M., Jiang W., Lu Z.-T., Yang G.-M. and Zhao L. (2019) Dual Separation of krypton and argon from environmental samples for radioisotope dating. *Anal. Chem.* **91**, 13576–13581.

Du X., Purtschert R., Bailey K., Lehmann B. E., Lorenzo R., Lu Z. T., Mueller P., O'Connor T. P. and Sturchio N. C. (2003) A new method of measuring ^{81}Kr and ^{85}Kr abundances in environmental samples. *Geophys. Res. Lett.* **30**, 2068.

Dwyer G. (1993) The Geology of the Welkom Goldfield with Special Reference to the a,b and Beatrix Reefs Exploration Geology. Rhodes University, p. 100.

Fabryka-Martin J. T. (1988) Production of Radionuclides in the Earth and their Hydrogeologic Significance, with Emphasis on Chlorine-36 and Iodine-129. Department of Hydrology and Water Resources, University of Arizona, p. 399.

Feige Y., Oltman B. and Kastner J. (1968) Production rates of neutrons in soils due to natural radioactivity. *J. Geophys. Res.* **73**, 3135–3142.

Florkowski T. (1992a) Natural Production of Radioactive Noble Gases in the Geosphere, Isotopes of Noble Gases as Tracers in Environmental Studies. IAEA, Vienna, pp. 11–27.

Florkowski T. and IAEA (1992b) Some aspects of the underground production of radionuclides used for dating groundwater. In *Isotope Techniques in Water Resource Development 1991*. IAEA, Vienna, pp. 215–228.

Florkowski T., Morawska L. and Rozanski K. (1988) Natural production of radionuclides in geological formations. *Nucl. Geophys.* **2**, 1.

Frimmel H. E., Groves D. I., Kirk J., Ruiz J., Chesley J., Minter W. E. L., Hedenquist J. W., Thompson J. F. H., Goldfarb R. J. and Richards J. P. (2005) The formation and preservation of the Witwatersrand Goldfields, the World's Largest Gold Province, One Hundredth Anniversary Volume. *Soc. Econ. Geol.*.

Fuchs S. H. J., Schumann D., Williams-Jones A. E., Murray A. J., Couillard M., Lagarec K., Phaneuf M. W. and Vali H. (2017) Gold and uranium concentration by interaction of immiscible fluids (hydrothermal and hydrocarbon) in the Carbon Leader Reef, Witwatersrand Supergroup, South Africa. *Precambr. Res.* **293**, 39–55.

Gerber C., Vaikmäe R., Aeschbach W., Babre A., Jiang W., Leuenberger M., Lu Z.-T., Mokrik R., Müller P., Raidla V., Saks T., Waber H. N., Weissbach T., Zappala J. C. and Purtschert R. (2017) Using ^{81}Kr and noble gases to characterize and date groundwater and brines in the Baltic Artesian Basin on the one-million-year timescale. *Geochim. Cosmochim. Acta* **205**, 187–210.

Heard A. W., Warr O., Borgonie G., Linage B., Kuloyo O., Fellowes J. W., Magnabosco C., Lau M. C. Y., Erasmus M., Cason E. D., van Heerden E., Kieft T. L., Mabry J. C., Onstott T. C., Sherwood Lollar B. and Ballentine C. J. (2018) South African crustal fracture fluids preserve paleometeoric water signatures for up to tens of millions of years. *Chem. Geol.* **493**, 379–395.

James M. F., Mills R. W. and Weaver D. R. (1991) A new evaluation of fission product yields and the production of a new library (UKFY2) of independent and cumulative yields. *Prog. Nucl. Energy* **26**, 1–29.

Jiang W., Bailey K., Lu Z. T., Mueller P., O'Connor T. M., Chen C. F., Hu S.-M., Purtschert R., Sturchio N. C., Sun Y. R., Williams W. D. and Yang G.-M. (2012) An atom counter for measuring ^{81}Kr and ^{85}Kr in environmental samples. *Geochem. Cosmochem. Acta* **91**, 1–6.

Jiang W., Hu S.-M., Lu Z.-T., Ritterbusch F. and Yang G.-M. (2020) Latest development of radiokrypton dating – A tool to find and study paleogroundwater. *Quat. Int.* **547**, 166–171.

Lau M. C. Y., Kieft T. L., Kuloyo O., Linage-Alvarez B., van Heerden E., Lindsay M. R., Magnabosco C., Wang W., Wiggins J. B., Guo L., Perlman D. H., Kyin S., Shwe H. H., Harris R. L., Oh Y., Yi M. J., Purtschert R., Slater G. F., Ono S., Wei S., Li L., Sherwood Lollar B. and Onstott T. C. (2016) An oligotrophic deep-subsurface community dependent on syntrophy is dominated by sulfur-driven autotrophic denitrifiers. *Proc. Natl. Acad. Sci.* **113**, E7927–E7936.

Lee J.-Y., Marti K., Severinghaus J. P., Kawamura K., Yoo H.-S., Lee J. B. and Kim J. S. (2006) A redetermination of the isotopic abundances of atmospheric Ar. *Geochim. Cosmochim. Acta* **70**, 4507–4512.

Lehmann B., Davis S. and Fabryka Martin J. (1993) Atmospheric and subsurface sources of stable and radioactive nuclides used for groundwater dating. *Water Resour. Res.* **29**, 2027–2040.

Lehmann B. E. and Purtschert R. (1997) Radioisotope dynamics; the origin and fate of nuclides in groundwater. *Appl. Geochem.* **12**, 727–738.

Lehmann B. E., Purtschert R., Collon P., Loosli H. H., Kutschera W., Love A., Beyerle U., Aeschbach-Hertig W., Kipfer R., Frape S. K., Herczeg A., Moran J., Tolstikhin I. N. and Gröning M. (2003) ^{81}Kr-A comparision of groundwater dating with ^{81}Kr, ^{36}Cl and ^{4}He in 4 wells of the Great Artesian Basin, Australia. *Earth Planet. Sci. Lett.* **211**, 237–250.

Leya I. and Wieler R. (1999) Nucleogenic production of Ne isotopes in Earth's crust and upper mantle induced by alpha particles from the decay of U and Th. *J. Geophys. Res. Solid Earth* **104**, 15439–15450.

Li J., Pang Z., Yang G.-M., Tian J., Tong A. L., Zhang X.-Y. and Hu S.-M. (2017) Million-year-old groundwater revealed by krypton-81 dating in Guanzhong Basin, China. *Sci. Bull.* **62**, 1181–1184.

Lippmann-Pipke J., Sherwood Lollar B., Niedermann S., Stroncik N. A., Naumann R., van Heerden E. and Onstott T. C. (2011) Neon identifies two billion year old fluid component in Kaapvaal Craton. *Chem. Geol.* **283**, 287–296.

Lippmann J., Stute M., Torgersen T., Moser D. P., Hall J. A., Lin L., Borcsik M., Bellamy R. E. S. and Onstott T. C. (2003) Dating ultra-deep mine waters with noble gases and ^{36}Cl, Witwatersrand Basin, South Africa. *Geochim. Cosmochim. Acta* **67**, 4597–4619.

Loosli H. H., Lehmann B. E. and Balderer W. (1989) Argon-39, argon-37 and krypton-85 isotopes in Stripa groundwaters. *Geochim. Cosmochim. Acta* **53**, 1825–1829.

Loosli H. H. and Purtschert R. (2005) Rare gases. In *Isotopes in the Water Cycle: Past, Present and Future of a Developing Science* (eds. P. Aggarwal, J. R. Gat and K. Froehlich). IAEA, Vienna, pp. 91–95.

Love A. J., Herczeg A. L., Sampson L., Cresswell R. G. and Fifield L. K. (2000) Sources of chloride and implications for ^{36}Cl dating of old groundwater, southwestern Great Artesian Basin, Australia. *Water Resour. Res.* **36**, 1561–1574.

Lu Z. T., Schlosser P., Smethie, Jr, W. M., Sturchio N. C., Fischer T. P., Kennedy B. M., Purtschert R., Severinghaus J. P., Solomon D. K., Tanhua T. and Yokochi R. (2014) Tracer applications of noble gas radionuclides in the geosciences. *Earth Sci. Rev.*.

Matsumoto T., Chen Z., Wei W., Yang G.-M., Hu S.-M. and Zhang X. (2018) Application of combined ^{81}Kr and ^{4}He chronometers to the dating of old groundwater in a tectonically active region of the North China Plain. *Earth Planet. Sci. Lett.* **493**, 208–217.

Mossman D., Minter W., Dutkiewicz A., Hallbauer D., George S., Hennigh Q., Reimer T. and Horscroft F. (2008) The indigenous origin of Witwatersrand "carbon". *Precambrian Res.* **164**, 173–186.

Munro D. D. (2013) Incline caving as a massive mining method. *J. South Afr. Inst. Min. Metall.* **113**, 555–563.

Nicolaysen L. O., Hart R. J. and Gale N. H. (1981) The Vredefort radioelement profile extended to supracrustal strata at Carletonville, with implications for continental heat flow. *J. Geophys. Res. Solid Earth* **86**, 10653–10661.

Nwaila G., Frimmel H. E. and Minter W. E. L. (2017) Provenance and Geochemical Variations in Shales of the Mesoarchean Witwatersrand Supergroup. *J. Geol.* **125**, 399–422.

Onstott T. C., Lin L.-H., Davidson M., Mislowac B., Borcsik M., Hall J., Slater G., Ward J., Sherwood Lollar B., Lippmann-Pipke J., Boice E., Pratt L., Pfiffner B. S., Moser D., Gihring T., Kieft T. L., Phelps T. J., van Heerden E., Litthauer D., DeFlaun M., Rothmel R., Wanger G. and Southham G. (2006) The origin and age of biogeochemical trends in deep fracture water of the Witwatersrand basin, South Africa. *Geomicrobiol. J.* **26**, 269–414.

Paul M., Tessler M. and Palchan T., et al. (2017) Nucleosynthesis reactions with the high-intensity Saraf-lilit neutron source. *The 26th International Nuclear Physics Conference*.

Pearson, Jr., F. J., Balderer W., Loosli H. H., Lehmann B. E., Matter A., Peters T., Schmassmann H. and Gautschi A. (1991) *Applied Isotope Hydrogeology a Case Study in Northern Switzerland*. Elsevier, Amsterdam, p. 439.

Phillips F. (2000) Chlorine-36. In *Environmental Tracers in Subsurface Hydrology* (eds. P. G. Cook and A. L. Herczeg). Kluwer, Boston, pp. 379–396.

Phillips F. M., Bentley H. W., Davis S. N., Elmore D. and Swanick G. B. (1986) Chlorine 36 dating of very old groundwater 2. Milk River Aquifer, Alberta, Canada. *Water Resour. Res.* **22**, 2003–2016.

Purtschert R., Sturchio N. C. and Yokochi R. (2013) Krypton-81 dating of old groundwater. In *Isotope Methods for Dating Old Groundwater* (eds. A. Suckow, P. Aggarwal and L. Araguas-Araguas). IAEA, Vienna, pp. 91–124.

Riedmann R. A. and Purtschert R. (2016) Separation of argon from environmental samples for Ar-37 and Ar-39 analyses. *Sep. Purif. Technol.* **170**, 217–223.

Rodney F. T., Richard P. V. and Morris J. V. (2016) A review of the Witwatersrand basin – the world's greatest goldfield. *Int. Union Geol. Sci.* **39**, 104–133.

Rozanski K. and Florkowski T. (1978) Krypton-85 dating of groundwater. In *Isotope Hydrology* (ed. IAEAIAEA). IAEA, Neuherberg, pp. 949–961.

Silver B. J., Raymond R., Sigman D. M., Prokopeko M., Sherwood Lollar B., Lacrampe-Couloume G., Fogel M. L., Pratt L. M., Lefticariu L. and Onstott T. C. (2012) The origin of NO3− and N2 in deep subsurface fracture water of South Africa. *Chem. Geol.* **294–295**, 51–62.

Singh B. and Chen J. (2014) Nuclear data sheets for A=85. *Nucl. Data Sheets* **116**, 1–162.

Slater G. F., Lippmann-Pipke J., Moser D. P., Reddy C. M., Onstott T. C., Lacrampe-Couloume G. and Lollar B. S. (2006) ^{14}C in methane and DIC in the deep terrestrial subsurface: implications for microbial methanogenesis. *Geomicrobiol. J.* **23**, 453–462.

Šrámek O., Stevens L., McDonough W. F., Mukhopadhyay S. and Peterson R. J. (2017) Subterranean production of neutrons, ^{39}Ar and ^{21}Ne: Rates and uncertainties. *Geochim. Cosmochim. Acta* **196**, 370–387.

Sturchio N. and Purtschert R. (2013) Krypton-81 case study: the Nubian aquifer, Egypt. In *Isotope Methods for Dating Old Groundwater* (ed. P. Aggarwal). IAEA, pp. 319–324.

Sturchio N. C., Du X., Purtschert R., Lehmann B., Sultan M., Patterson L. J., Lu Z.-T., Müller P., Bigler T., Bailey K., O'Connor T. P., Young L., Lorenzo R., Becker R., El Alfy Z., El Kaliouby B., Dawood Y. and Abdallah A. M. A. (2004) One million year old groundwater in the Sahara revealed by krypton-81 and chlorine-36. *Geophys. Res. Lett.* **31**, L05503.

Sturchio N. C., Kuhlman K. L., Yokochi R., Probst P. C., Jiang W., Lu Z.-T., Mueller P. and Yang G.-M. (2014) Krypton-81 in groundwater of the Culebra Dolomite near the Waste Isolation Pilot Plant, New Mexico. *J. Contam. Hydrol.* **160**, 12–20.

Wahl A. C. (1958) Nuclear-charge distribution in fission: cumulative yields of short lived krypton and xenon isotopes from thermal neutron fission of ^{235}U. *J. Inorg. Nucl. Chem.* **6**, 263.

Wronkiewicz D. J. and Condie K. C. (1987) Geochemistry of Archean shales from the Witwatersrand Supergroup, South Africa: Source-area weathering and provenance. *Geochim. Cosmochim. Acta* **51**, 2401–2416.

Yatsevich I. and Honda M. (1997) Production of nucleogenic neon in the Earth from natural radioactive decay. *J. Geophys. Res. Solid Earth* **102**, 10291–10298.

Yechieli Y., Yokochi R., Zilberbrand M., Lu Z.-T., Purtschert R., Sueltenfuss J., Jiang W., Zappala J., Mueller P., Bernier R., Avrahamov N., Adar E., Talhami F., Livshitz Y. and Burg A. (2019) Recent seawater intrusion into deep aquifer determined by the radioactive noble-gas isotopes ^{81}Kr and ^{39}Ar. *Earth Planet. Sci. Lett.* **507**, 21–29.

Yokochi R. (2016) Recent developments on field gas extraction and sample preparation methods for radiokrypton dating of groundwater. *J. Hydrol.* **540**, 368–378.

Yokochi R., Ram R., Zappala J. C., Jiang W., Adar E., Bernier R., Burg A., Dayan U., Lu Z.-T., Mueller P., Purtschert R. and Yechieli Y. (2019) Radiokrypton unveils dual moisture sources of a deep desert aquifer. *Proc. Natl. Acad. Sci.* **116**, 16222.

Yokochi R., Sturchio N. C. and Purtschert R. (2012) Determination of crustal fluid residence times using nucleogenic ^{39}Ar. *Geochem. Cosmochem. Acta* **88**, 19–26.

Zappala J. C., Baggenstos D., Gerber C., Jiang W., Kennedy B. M., Lu Z. T., Masarik J., Mueller P., Purtschert R. and Visser A. (2020) Atmospheric ^{81}Kr as an integrator of cosmic-ray flux on the hundred-thousand-year timescale. *Geophys. Res. Lett.*, e2019GL086381.

Associate editor: Anthony Dosseto